Sensor and Simulation Notes

Note 545

October 25, 2009

Radiation Patterns of a Reflector Type of Impulse Radiating Antenna (IRA) Relating Time and Frequency Domains

K. Sunitha
Pulsed Power and EMC Laboratory
Department of Electrical Engineering
Indian Institute of Science, Bengaluru- 560012, INDIA

Dr. D. V. Giri
Pro-Tech, 11 C Orchard Court, Alamo, CA 94507-1541
Dept. of Electrical and Computer Engg., Univ. of New Mexico, Albuquerque, NM 87131

and

Prof. M. Joy Thomas
Pulsed Power and EMC Laboratory
Department of Electrical Engineering
Indian Institute of Science, Bengaluru-560012, INDIA

Abstract

In this note, we have addressed the problem of computing the field radiation patterns of an IRA using the aperture field integration method. There is a transformable relationship between the spectral and temporal radiation patterns of an IRA, which is sometimes mis-understood. The essence of this equivalence is contained in Fourier or Laplace transformation. At any arbitrary observation point in front of an IRA, one can measure a temporal electric field. This temporal field can be represented as a sum of sinusoidal signals of varying frequencies, amplitudes and phases. We have outlined a method of computing the radiation patterns at a given frequency and applied this to the prototype IRA over a very broad range of frequencies.

1. Introduction

In the 1960's, frequency-independent antennas were the rage. Log-periodic, spiral and conical-log spiral antennas were introduced by Rumsey and others, and Prof. R. DuHamel was investigating ways of feeding lens and reflector antennas in such a way that they could also operate over a large frequency range. In an early paper presented in an IEEE APS Symposium [1], DuHamel and his co-authors describe an innovative antenna design for this purpose. This antenna consisted of a paraboloidal reflector fed by several wires starting from the focal point, without any terminating resistors at the end of the wires Unfortunately, as far as one can tell from a literature search, this antenna design by DuHamel was never pursued and used in antenna applications. In 1989 Baum independently conceived of a broad-band antenna concept, which he referred to as the "Impulse Radiating Antenna", or IRA [2]. Baum [2] also introduced appropriate terminations in the transmission-line feed and a transmission line balun so that the antenna can be matched to a 50 Ohm source. Proper termination of the feed line results in improved low-frequency performance of the antenna [2]. This concept was developed for the purpose of being able to simulate transient EM fields at a target for a wide variety of applications – including defense and civilian applications.

Subsequent investigations into the radiating properties of the IRA [3 to 6] show that it is possible to design a reflector-style antenna that can operate in a phase coherent manner over several decades in frequency. Within the operating band of the IRA, the radiated field from the antenna is almost a linear function of frequency, implying that the radiated field in the time domain looks like the derivative of the applied transient voltage source driving the antenna. Hence, if a step function voltage were applied to the antenna, the radiated E-field at a distance would appear similar to a delta function in time. Of course, the step function response of the IRA would not be an exact impulse function. Because an antenna cannot radiate DC into the far field, any waveform produced from this antenna at a distant observation point must have zero area, which precludes the impulse function. The actual radiated field from the IRA for a step function excitation is reminiscent of the delta function, but has a zero net area. Thus, this transient waveform is referred to as being "impulse-like."

In this paper, our focus is on computing the field radiation pattern of the IRA at various frequencies and then comment on the equivalence between time and frequency domain responses.

2. Aperture Integration Method

2.1 Uniform Aperture Field

A paraboloidal reflector is an aperture antenna. If this aperture had a constant E-field denoted by E_a, the far field is simply given by an integration of the aperture field over the aperture. If A is the area of this aperture and r is the boresight range and λ is the wavelength of the mono-chromatic illumination, the far field is given by a very simple relationship

$$E_{far}(r,\lambda) = \left|\frac{E_a A}{r\lambda}\right| = \left|\frac{\omega E_a A}{2\pi r c}\right| \quad or \quad \left(\frac{E_{far}}{E_a}\right) = \left(\frac{A}{r\lambda}\right) = \left(\frac{\omega A}{2\pi r c}\right) \tag{1}$$

where c is the speed of light in vacuum. This simple equation demonstrates the differentiating character of an aperture. In other words, the far field is a spatial integration of the aperture field combined with its temporal derivative, since $(j\omega)$ in frequency domain translates to $(\partial / \partial t)$ in time domain. Clearly, a step function aperture field results in an impulse-like far field with its rich hyperband [7] characteristics. Thus an intimate knowledge of the aperture fields is both sufficient and necessary in computing the far fields.

The gain of an aperture antenna with a ***uniform aperture field*** can be easily derived.

$$G_u(\theta,\phi) = Lim(r \to \infty)\ 4\pi r^2 \frac{S(r,\theta,\phi)}{P_{in}}$$
$$S(r,\theta,\phi) = \frac{1}{2}\mathrm{Re}(\vec{E}\, x\, \vec{H}^*) = \frac{1}{2Z_o} E^2 \quad Watts/m^2 \qquad (2)$$
$$P_{in} = \frac{1}{2}\mathrm{Re}(E_a\, x\, H_a^*) = \frac{1}{2}(\pi a^2)\frac{E_a^2}{Z_o} \quad Watts$$

Directive Gain becomes

$$G_u = Lim(r \to \infty)\left[4\pi r^2\right]\left(\frac{E^2}{2Z_o}\right)\left(\frac{2Z_o}{\pi a^2 E_a^2}\right) = Lim(r \to \infty)\left(\frac{4}{a^2}\right)\left[\frac{r\,E}{E_a}\right]^2 \qquad (3)$$

In the far field $(r \to \infty)$, equation (1) gives $\frac{rE}{E_a} = \frac{\omega A}{2\pi c} = \frac{A}{\lambda}$ (4)

The directive gain simplifies to

$$G_u = \left(\frac{4A^2}{a^2\lambda^2}\right) = \left(\frac{\pi^2 D^2}{\lambda^2}\right);\ G(indB) = 10\log_{10}\left(\frac{\pi^2 D^2}{\lambda^2}\right)\ with D = aperture diamter \qquad (5)$$

This would be the highest gain one could obtain for a perfect aperture. We will now proceed to investigate the radiation patterns and the gain of a 2–arm and a 4-arm IRA.

We can now consider the geometry of a paraboloidal reflector antenna shown in figure 1. We follow the aperture integration method outlined by Balanis [8].

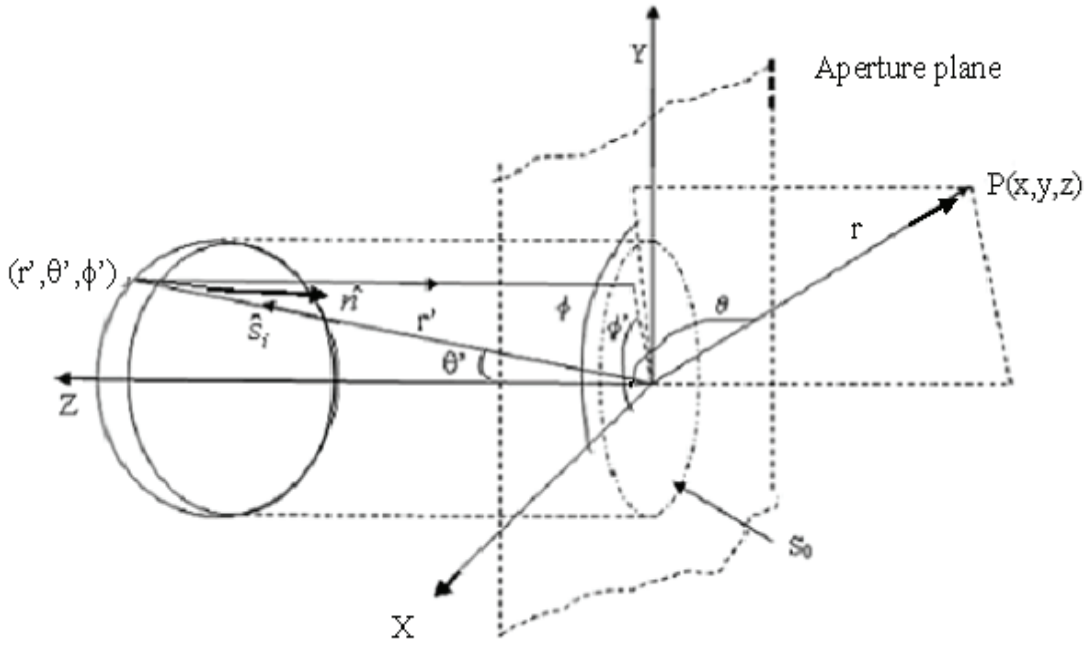

Figure 1. Reflector geometry and the aperture plane

For the given source at the focal point, let the gain function be $G_f(\theta',\phi')$. Then the radiation intensity is given by

$$U(\theta',\phi') = \frac{P_t}{4\pi} G_f(\theta',\phi') \tag{6}$$

where P_t is the total radiated power. The incident field, with the direction perpendicular to the radial distance, can be written as

$$\mathbf{E_i}(r',?',f') = \hat{e}_i \; C_1 \sqrt{G_f(\theta',\phi')} \; \frac{e^{-jkr'}}{r'} \tag{7}$$

where the unit vectors are as shown in figure 2.

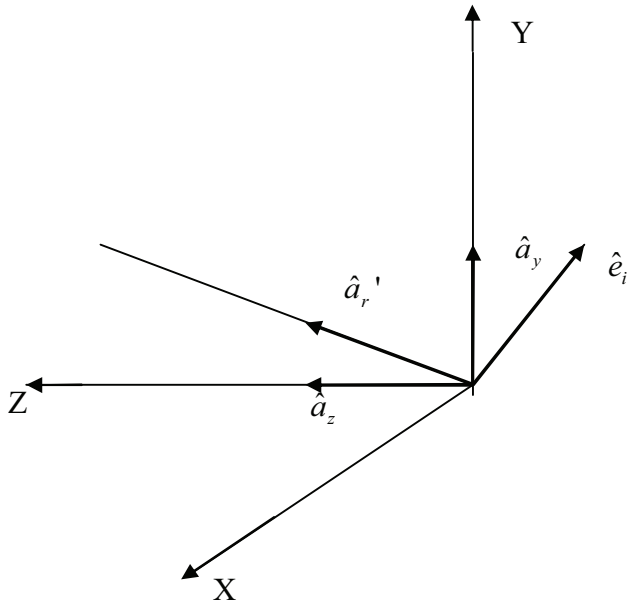

Figure 2. Orientations of the various unit vectors

On the surface of the reflector the current density vector is given by

$$\mathbf{J}_s = 2\sqrt{\frac{\varepsilon}{\mu}} C_1 \sqrt{G_f(\theta',\phi')}\ \frac{e^{-jkr'}}{r'}\mathbf{u} \tag{8}$$

where

$$\mathbf{u} = [-\hat{a}_x \sin\theta' \sin\left(\frac{\theta'}{2}\right)\sin\phi' \cos\phi' + \hat{a}_y \cos\left(\frac{\theta'}{2}\right)(\sin^2\phi'\cos\theta' + \cos^2\phi')$$
$$- \hat{a}_z \cos\theta' \sin\left(\frac{\theta'}{2}\right)\sin\phi'\cos\phi'] \,/\, \sqrt{1-\sin^2\theta'\sin^2\phi'} \tag{9}$$

and

$$C_1 = \left(\frac{\mu}{\varepsilon}\right)^{\frac{1}{4}}\left(\frac{P_t}{2\pi}\right)^{\frac{1}{2}} \tag{10}$$

To find the aperture field at a plane through the focal point, the reflected fields $\mathbf{E_r}$ at r' is first found. This is of the form

$$\mathbf{E_r} = \hat{e}_r\ C_1 \sqrt{G_f(\theta', \phi')}\ \ \frac{e^{-jkr'}}{r'} \tag{11}$$

where $\hat{e}_r$ is the unit vector depicting the polarization of the field. The current density vector for the reflected field is

$$\mathbf{J}_s = 2\sqrt{\frac{\varepsilon}{\mu}} C_1 \sqrt{G_f(\theta',\phi')}\ \frac{e^{-jkr'}}{r'}\mathbf{u} \tag{12}$$

where $\mathbf{u} = \hat{n}\times(-\hat{a}_z \times \hat{e}_r)$

And the vector $\hat{n}$ is shown in figure1. For the given geometry $\hat{e}_r$ becomes

$$\hat{e}_r = \frac{[\hat{a}_x \sin\phi' \cos\phi'(1-\cos\theta') - \hat{a}_y (\sin^2\phi'\cos\theta' + \cos^2\phi')]}{\sqrt{1-\sin^2\theta'\sin^2\phi'}} \tag{13}$$

Hence on any plane passing through the focal point, the reflected field is given by

$$\mathbf{E_{ap}} = \hat{e}_r\ C_1 \sqrt{G_f(\theta',\phi')}\ \ \frac{e^{-jkr'(1+\cos\theta')}}{r'(1+\cos\theta')} = \hat{a}_x E_{xa} + \hat{a}_y E_{ya} \tag{14}$$

where E_{xa} and E_{ya} are the x and y components of the reflected field. So on the aperture the current density vector will be

$$\mathbf{J_s} = -\hat{a}_x \frac{E_{ax}}{\eta} - \hat{a}_y \frac{E_{ay}}{\eta} \tag{15}$$

where η is the intrinsic impedance of the medium. The equivalent magnetic current is given by

$$\mathbf{M_s} = \hat{a}_x E_{ay} - \hat{a}_y E_{ax} \tag{16}$$

From the general radiation equation we can write at any observation point at a distance r from the focal point as shown in figure 1

$$E_{\theta s} = \frac{-jke^{-jkr}}{4\pi r}(L_\phi + \eta N_\theta) \tag{17}$$

where

$$L_\phi = \iint_{S_0} [-M_x \sin\phi + M_y \cos\phi] e^{+jkr'\cos\psi}\, ds' \tag{18}$$

$$N_\theta = \iint_{S_0} [J_x \cos\theta\cos\phi + J_y \cos\theta\sin\phi - J_z \sin\theta] e^{+jkr'\cos\psi}\, ds' \tag{19}$$

where ψ is the angle between r and r' . The orientations of the various unit vectors are shown in figure 2.

Hence the net radiated field on the aperture is given by

$$E_{\theta s} = \frac{jke^{-jkr}}{4\pi r}(1+\cos\theta)\iint_{S_0}(E_{ax}\cos\phi + E_{ay}\sin\phi)e^{jk(x'\sin\theta\cos\phi + y'\sin\theta\sin\phi)}\,dx'\,dy' \tag{20}$$

r is the radial distance to the observation point θ and ϕ are the angular coordinates of the observation point as shown in figure 1. This expression is accurate in the forward direction, but seems to give reasonable estimates even in the backward direction. If needed, one can also explicitly write down the rectangular components of the field at any arbitrary observation point. For now, we have chosen to work with the theta component.

3. Illustrative Example in Frequency Domain

A prototype IRA [4] has been considered and is shown in figure 3.

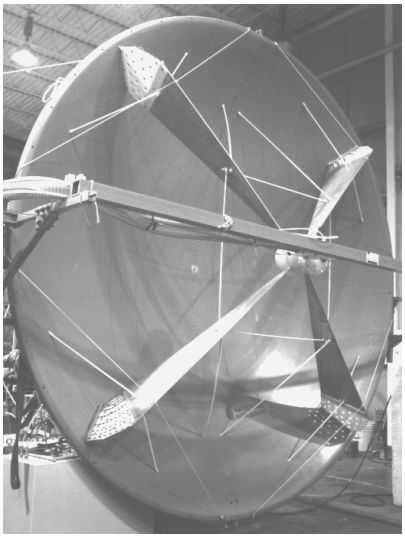

Figure 3. Prototype IRA (D = 3.66m and F/D = 0.33)

In our computations, we assume ϕ to be a constant and the resultant variation of the field with respect to θ is estimated using equation 20. The field is plotted as a normalized field of the maximum electric field intensity occurring along the boresight. The integration is done numerically in MATLAB along the x and y coordinates of the aperture plane. The calculations of the radiated electric field (theta component) patterns from equation (16) have been performed at spot frequencies of 1 MHz, 100 MHz, 200 MHz, 500MHz, 1GHz, 4 GHz and 10 GHz. The frequency range is seen to be extending from Medium Frequency (MF) to X-band.

The computed field radiation patterns at various frequencies are shown in figures 4 to 6.

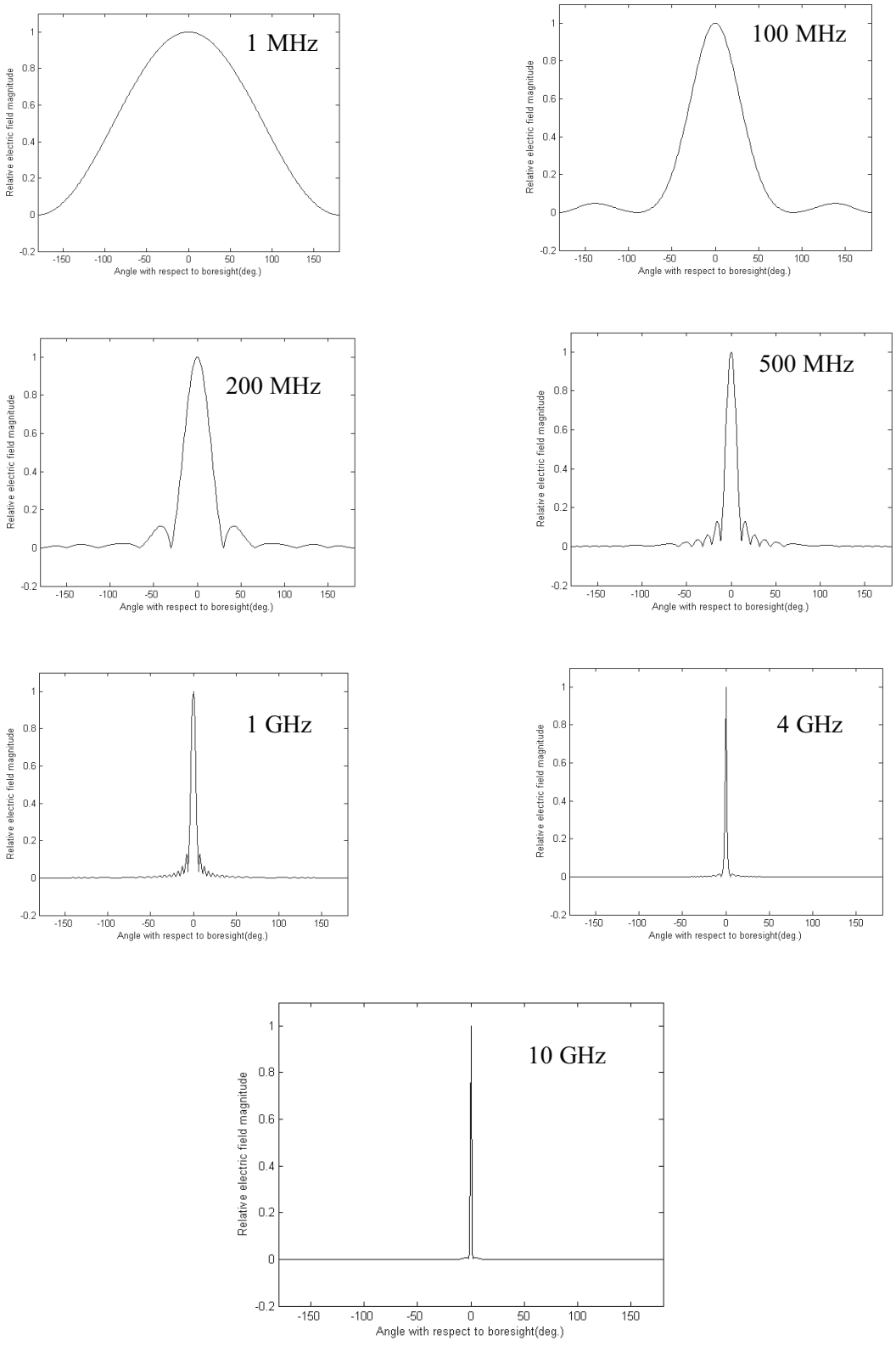

Figure 4. Normalized field at different frequencies as a function of angle off boresight

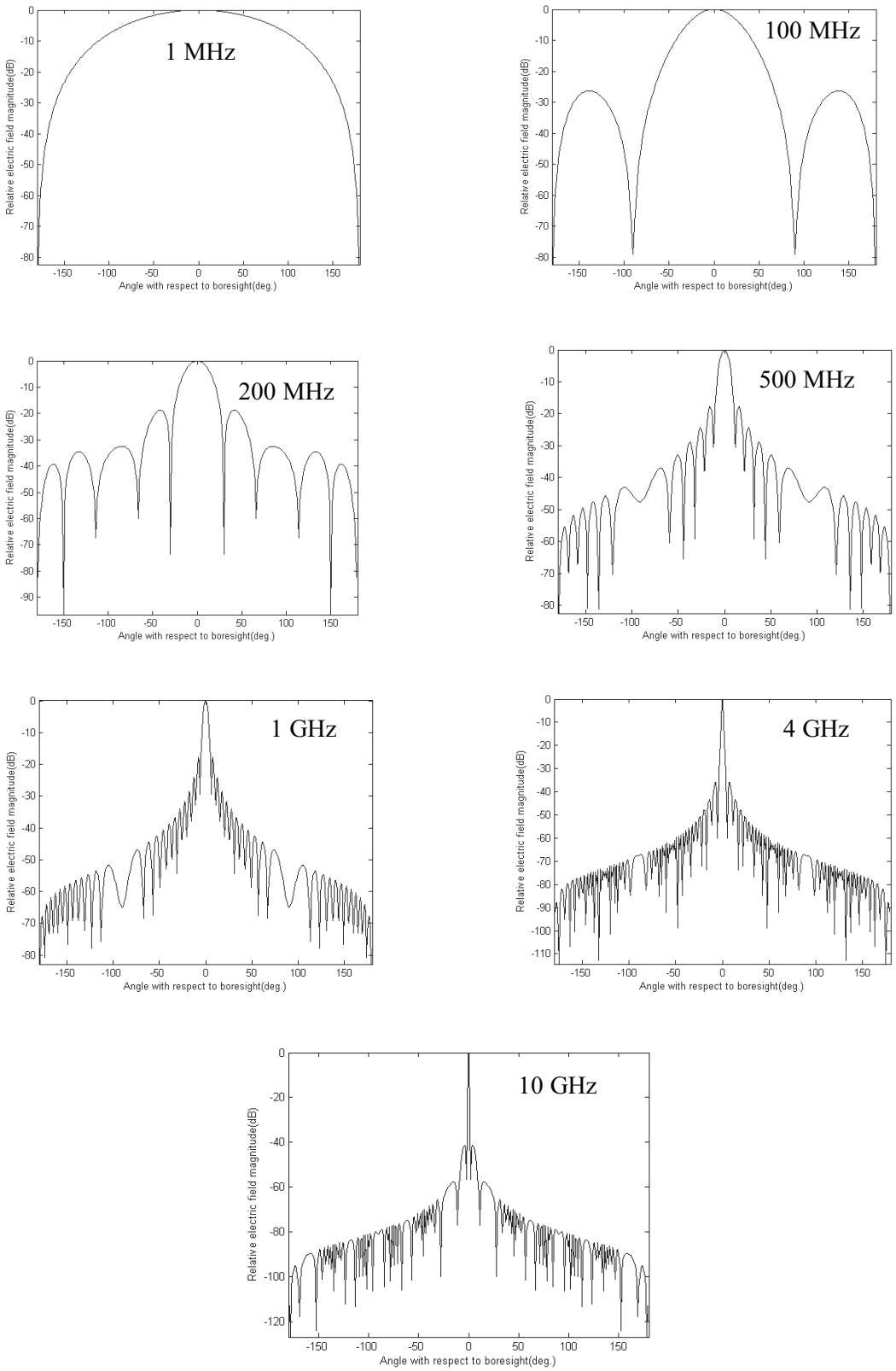

Figure 5. Field pattern in dB at different frequencies as a function of angle off boresight

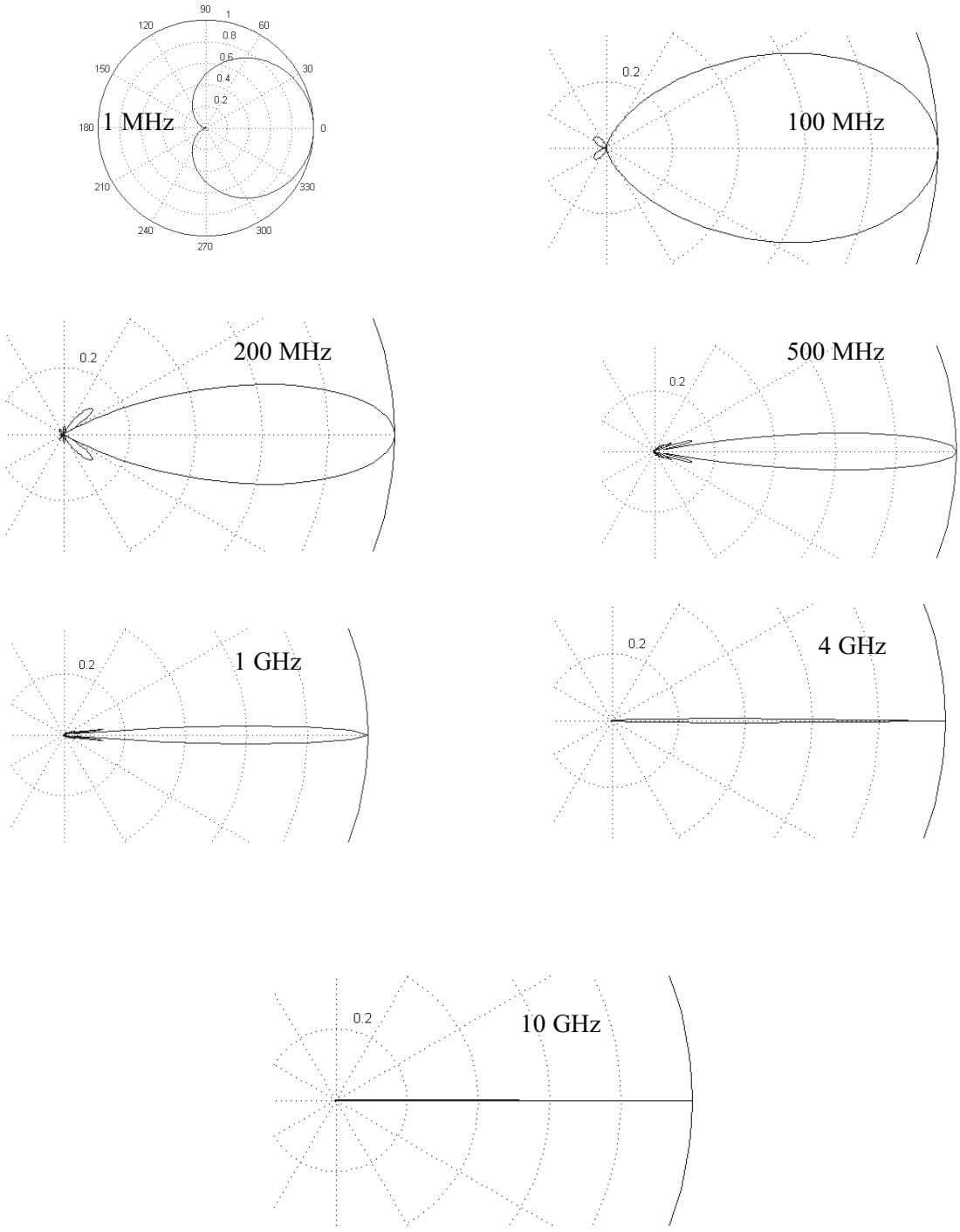

Figure 6. Polar plot of the field radiation pattern at various frequencies

The wavelengths where computations have been made are 300m, 3m, 1.5m, 60cm, 30cm, 7.5 cm and 3 cm. The antenna diameter D in terms of wavelength (D/λ) has the values of 0.012, 1.221, 2.442, 6.105, 12.21, 48.84, 122.1. At the very low-frequency of 1 MHz, one would expect the radiation pattern to be that of a dual dipole ($(\vec{p}\,x\,\vec{m})$ with a near cardioid pattern that has a very broad beam width. One can also see this from equation (16), at very low frequencies, (kx' <<1), the integral becomes nearly a constant and the cardioid or [1+ cos (θ)] becomes apparent. The beam width decreases with frequency, as expected. The beam widths are shown in Table 1.

TABLE 1. Beam width as a function of frequency

Frequency (MHz)	Beam width (degrees)
1	131
100	47
200	24
500	9.5
1,000	4.8
4,000	0.88
10,000	0.55

It is evident that ***all*** the frequencies have their peak radiation on boresight. One can say this is somewhat fortuitous, since when this antenna was originally designed, we had not looked at the low frequency performance. Later analyses showed that the even at the very low frequencies where the antenna can be characterized by a pair of dipole moments (electric and magnetic), the resultant radiation is in the boresight direction.

The field patterns at various frequencies shown in figures 4, 5 and 6 are just that. They are not indicative of the relative strength of the fields at various frequencies, only the variation off boresight axis, after normalizing the fields to the peak value on boresight at each frequency. The relative strengths of each sinusoidal component and relative phases depends on many factors such as the excitation voltage spectrum, antenna size etc.

The *directive gain* or the gain along the boresight of the IRA as a function of frequency is easy to derive. Let us consider a 2-arm IRA, to begin with.

$$G(\theta,\phi) = Lim(r \to \infty)\ \ 4\pi r^2 \frac{S(r,\theta,\phi)}{P_{in}} \tag{21}$$

On boresight, we have

$$\begin{aligned} S(r,\theta,\phi) &= \frac{1}{2}\mathrm{Re}(\vec{E}\,x\,\vec{H}^*) = \frac{1}{2Z_o}E^2 \qquad Watts/m^2 \\ P_{in} &= \frac{1}{2}\mathrm{Re}(V_a\,x\,I_a^*) = \frac{1}{2Z_{in}}V_a^2 \qquad Watts \end{aligned} \tag{22}$$

Directive Gain becomes

$$G = Lim(r \to \infty)\left[\frac{4\pi Z_{in}}{Z_o}\right]\left[\frac{r\,E}{V_a}\right]^2 = Lim(r \to \infty)\left(4\pi f_{g2}\right)\left[\frac{r\,E}{V_a}\right]^2 \tag{23}$$

In the far field $(r \to \infty)$, $\quad \frac{r\,E}{V_a} = \frac{D\omega}{4\pi c\, f_{g2}} = \frac{D}{2\lambda f_{g2}}$ (24)

The directive gain simplifies to

$$G = \left(\frac{\pi\ D^2}{f_{g2}\,\lambda^2}\right);\ G(in\,dB) = 10\log_{10}\left(\frac{\pi\ D^2}{f_{g2}\,\lambda^2}\right) with\ D = reflector\ diamter\ \ and\ \ f_{g2} = \frac{Z_{in}}{Z_o} \tag{25}$$

For a 2-arm IRA, the numerical parameters are D =3.66m and f_{g2} = 400 Ohms/376.98 Ohms = 1.061, and we have listed the directive gain in Table 2.

TABLE 2. Estimated directive gain v. frequency for a 2-arm IRA (same as 4-arm IRA)

freq	wavelength	D/λ	Directive Gain (Numerical)	Directive Gain (dB)
1MHz	300 m	0.012	0.00044	- 33.56 dB
100 MHz	3 m	1.221	0.8222	- 0.85 dB
200 MHz	1.5 m	2.442	18.17	12.59 dB
500 MHz	60 cm	6.105	111.7	20.48 dB
1 GHz	30 cm	12.21	454.2	26.57 dB
4 GHz	7.5 cm	48.84	7,268	38.61 dB
10 GHz	3 cm	122.1	45,425	46.57 dB

The directive gain is seen to increase as (frequency)^2 or 20 dB per decade. In practice, however, the gain does not arbitrarily increase and will cut off at some high frequency due to feed imperfections.

We also observe that for a 4-arm IRA, the radiated field is larger by a factor of $\sqrt{2}$ resulting in twice the radiated power of a 2-arm IRA. However, the input power is also increased by a factor of 2. Consequently, the directive gain remains unchanged. We have summarized the gains of the aperture antennas considered in this paper in Table 3.

TABLE 3. Directive Power Gain of the aperture antennas

Type of Aperture Antenna	**Directive Power Gain**
A circular aperture (diameter D) with an uniform aperture field or the "perfect aperture"	$\pi^2\left(\frac{D^2}{\lambda^2}\right)$
2-arm IRA of diameter D Typically $f_{g2}=(400\Omega/376.98\Omega)=1.061$	$\left(\frac{\pi}{f_{g2}}\right)\left(\frac{D^2}{\lambda^2}\right)$
4-arm IRA of diameter D (90° feed arms) Directive Gain is same as the 2-arm case, since both the radiated and input powers are increased by a factor of 2. $\left(f_{g2}=2f_{g4}\right)$	$\left(\frac{2}{(f_{g2}/f_{g4})}\right)\left(\frac{\pi}{f_{g2}}\right)\left(\frac{D^2}{\lambda^2}\right)=\left(\frac{\pi}{f_{g2}}\right)\left(\frac{D^2}{\lambda^2}\right)$
4-arm IRA of diameter D (60° feed arms)	~ 20% higher than a 4-arm IRA (90° feed arms) or a 2-arm IRA

4. Illustrative Example in Time Domain

The prototype IRA reflector is fed by a transverse electromagnetic wave structure energized by a $\pm 60kV$ source. The detailed description of the source is available in [4, 5]. The characteristic properties of this antenna includes the far field electric field measured in the boresight at r = 305m being equal to 4.2kV/m, the uncorrected pulse rise time (10%-90%) equal to 99ps and the boresight electric field's FWHM equal to 130ps.

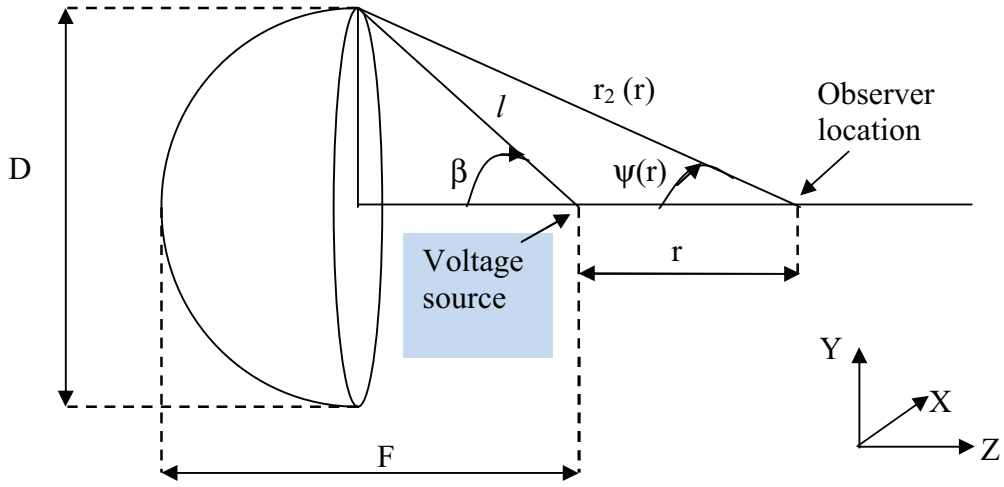

Figure 7. A parabolic reflector type IRA

The following analytical model has been used to describe the output voltage, according to which the pulser output voltage, its derivative and the Fourier Transform can be written as [5]

$$V(t)=\begin{cases} V_0 e^{-(\beta\,(t/t_d))}\left(\dfrac{1}{2}erfc\left(\sqrt{\pi}\,\dfrac{|t|}{t_d}\right)\right) & t<0 \\ V_0 e^{-(\beta\,(t/t_d))}\left(1-\dfrac{1}{2}erfc\left(\sqrt{\pi}\,\dfrac{|t|}{t_d}\right)\right) & t>0 \end{cases} \tag{26}$$

$$\tilde{V}(\omega)=\frac{V_0 t_d}{(\beta+j\omega t_d)}e^{\{(1/4\pi)(\beta+j\omega t_d)^2\}} \tag{27}$$

For the pulser feeding the IRA, these parameters are [5]

V_0 = 120.72kV $\quad t_d$ = 100ps $\quad \beta$ = 0.005 $\quad (dV/dt)_{max} = 1.2\text{x}10^{15}$ V/s. (28)

The peak amplitude of the voltage waveform is slightly less than V_0. We find that with V_0 of 120.72 kV, the peak amplitude turns out to be 120 kV. The above outlined model is depicted in the figure 7 for the voltage. This voltage is used for the computation of the electric field.

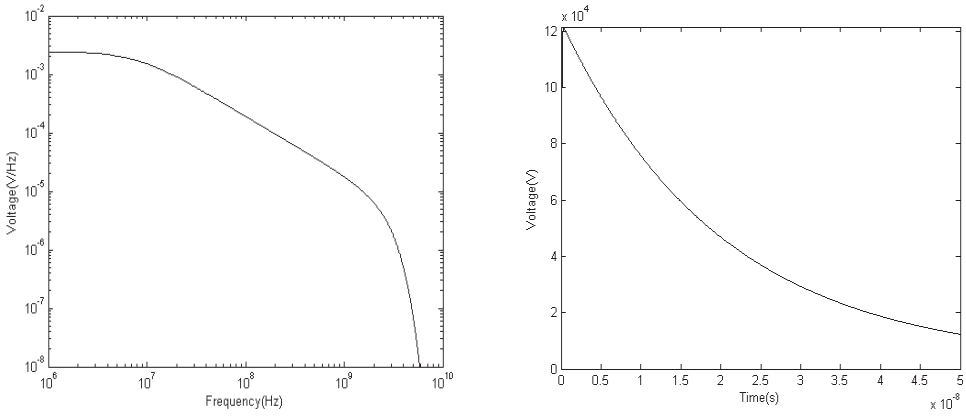

(a) (b)

Figure 7. Output voltage of the pulser (a) Frequency domain (b) time domain

One can compute the boresight temporal field at various distances using a closed form expression developed in [6]. It is also possible to calculate the fields in frequency domain as described in previous section and do an inverse Fourier transform to get temporal fields. The results are the same and the temporal fields are shown plotted in Figure 8, as computed from the aperture integration method of the previous section combined with Fourier inversion.

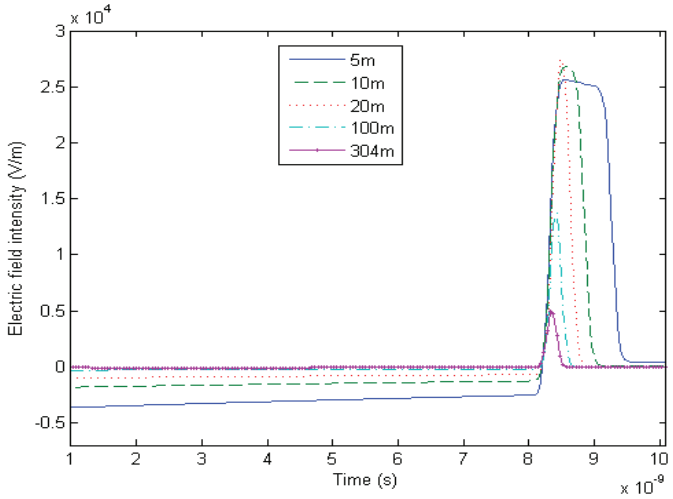

Figure 8. Electric field at different points along the boresight in time domain

The far field can be shown [5] to start at a range r given by

$$r \geq \frac{D^2}{2c\,t_r} \tag{29}$$

This range turns out to be about 225m and let us pick an observation point at a boresight range of 304m in the far field. The temporal and spectral magnitudes of the electric field at this

observation point are shown in figures 9. These estimates have been validated by measurements.

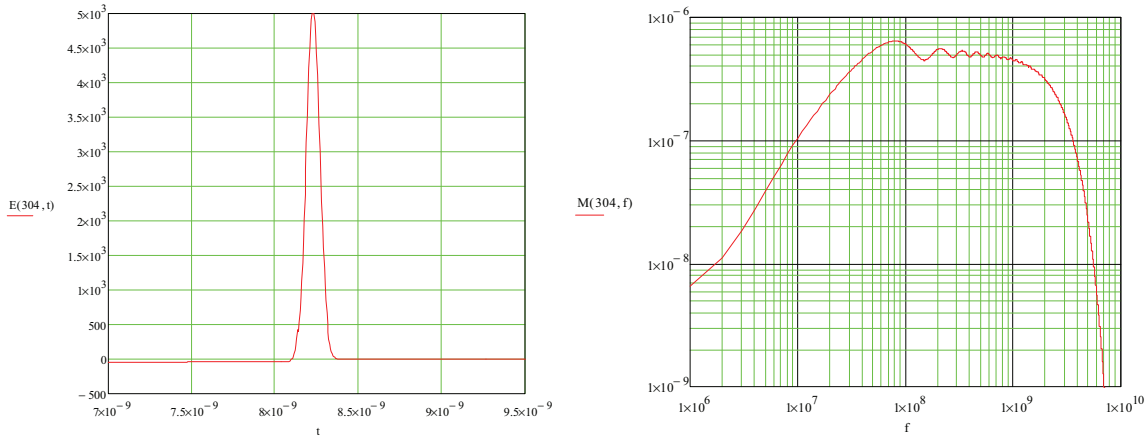

(a) (b)

Figure 9. Boresight field at 304 m; (a) temporal and (b) spectral magnitude

In the next section, we will discuss the equivalence between the temporal and spectral characteristics of the IRA that have been described in sections 3 and 4.

5. Equivalence between the Spectral and Temporal Characteristics of the IRA

The equivalence is based on the fundamental principle of Fourier or Laplace transformation. For simplicity, let us write the Fourier transform pair of integrals.

$$f(t) = \frac{1}{2\pi}\int_{-\infty}^{\infty} F(\omega) e^{j\omega t}\, d\omega \qquad F(\omega) = \int_{-\infty}^{\infty} f(t)\, e^{-j\omega t}\, dt \tag{30}$$

Note that $f(t)$ is a real function of a real variable t while $F(\omega)$ is a complex function of a real variable ω. One has to know the temporal function for ***all*** times to get the spectrum and conversely, one has to know the spectral function for ***all*** frequencies to get the temporal function. In measurement scenarios, this creates a problem since the data is either band limited or time limited. Nevertheless the equivalence is straight forward.

By setting $t = 0$ and $\omega = 0$, observe that

$$f(0) = \frac{1}{2\pi}\int_{-\infty}^{\infty} F(\omega)\, d\omega \quad \text{and} \quad F(0) = \int_{-\infty}^{\infty} f(t)\, dt \tag{31}$$

Both of these quantities (initial value in time domain and DC content in frequency domain) need to be = 0 if we are dealing with a radiated electric field. The reasons being; 1) there cannot be a radiated signal before the signal can get there and 2) antennas do not radiate DC

into the far field). Ensuring these vanishing quantities in a measurement can be a good check on the measurement schemes.

In the context of an IRA, we observe that it can be excited by a transient pulse that contains many frequencies or by a single frequency sinusoidal voltage. If we apply a CW sinusoidal voltage to the IRA, the far field is the derivative of the sinusoid or simply a co-sinusoid everywhere. What is changing with the observer location is the amplitude and phase of that co-sinusoid. The amplitude is changing with angle off the boresight for example, as we have estimated in Figures 4, 5 and 6 at various frequencies. The amplitude on boresight will depend on the values of antenna size, frequency and the antenna impedance.

If we use the IRA in a pulsed mode, the voltage pulse has many frequencies. They all get radiated from the same focal point of the reflector (hence the antenna is non-dispersive). However, each frequency has a different radiation pattern as we have computed in this paper. If we measure the radiated field at any arbitrary position in front of the antenna, we get a temporal waveform E(r, t), as in figure 9a for example. This E(r, t) has a definite relationship with the applied voltage. It is important to realize that the E(r, t) when Fourier transformed will have many frequencies with varying amplitudes and phases, as in figure 9b. Phase is a frequency domain concept and is equivalent to a delay in time domain. A time domain signal (radiated electric field in this case of figure 9a) is merely a collection of many sinusoids, each with a different amplitude and phase as shown in figure 9b.

Gain and beam-width of the IRA as calculated in section 3 varied with frequency. In time domain the precise definitions of gain and beam-width are yet to be standardized. We have chosen to define the temporal beam-width as the angular points where the peak power of the temporal waveforms is half of their boresight value. This is simply a matter of convenience at this time. Suffice it to say that in front of the pulse-excited IRA, one has a temporal waveform of the electric field at any arbitrary observation point and this waveform can be Fourier transformed to observe its spectral content. It does not make sense to talk of “side lobes” in time domain. One can also assert that the high frequencies have the highest directive gain and hence the pulse on boresight will have the shortest rise time. The radiated pulse becomes smaller and fatter as, one goes off the boresight.

It is likely that standardized definitions of Gain and Beam-width will evolve in the future for pulsed antennas.

References

1. R. H. DuHamel, M. B. Armstrong, J. J. Campbell, W. R. Jones, and W. F. Pedler, Frequency Independent Conical Feeds for Lens and Reflectors, *Proceedings of the IEEE APS Symposium*, 1968.

2. C. E Baum*, "Radiation of Impulse-Like Transient Fields," Sensor and Simulation Note 321*, 25 November 1989.

3. C. E.Baum and E.G. Farr, "Impulse Radiating Antennas," in Ultra-Wideband Short Pulse Electromagnetics, edited by H. L. Bertoni et al., pp 139-147, Plenum Press, NY 1993.

4. I. D. Smith, D. W. Morton, D. V. Giri, H. Lackner, C. E. Baum, J. R. Marek, " Design, Fabrication and Testing of a Paraboloidal Reflector Antenna and Pulser System for Impulse-Like Waveforms", *Proceedings of the Tenth IEEE International Pulsed Power Conference*, Albuquerque, NM, July 3-6, 1995, Vol. 1, pp 56-64. Also in *IEEE Trans Plasma Science*, April 1997, pp 318-326.

5. D. V. Giri, High-Power Electromagnetic Radiators: Nonlethal Weapons and Other Applications, Harvard University Press, November 2004.

6. Oleg V. Mikheev, et. al, "New Method for Calculating Pulse Radiation from an Antenna with a Reflector", *IEEE Trans. EMC*, February 1997.

7. D. V. Giri and F. M. Tesche, "Classification of Intentional Electromagnetic Environments", IEEE Transactions on Electromagnetic Compatibility, Special Issue on HPEM and IEMI, August 2004, pp 322-328

8. C. A. Balanis, *Antenna Theory Analysis and Design*, John Wiley & Sons, Publishers, Inc., New York, 2005.